processes

MDPI

Article

Experimental Study on the Spray Characteristics of Diesel and Hydrotreated Vegetable Oil (HVO) Fuels under Different Injection Pressures

Chang Zhai [1,2], Kuichun Li [2], Pengbo Dong [3], Yu Jin [4], Hongliang Luo [1,*], Beini Zhou [5] and Yang Liu [5]

[1] College of Power and Energy Engineering, Harbin Engineering University, Harbin 150001, China; chang.zhai@aist.go.jp
[2] Department of Mechanical System Engineering, University of Hiroshima, 1-4-1 Kagamiyama, Higashi-Hiroshima 739-8527, Japan; likuichun@gmail.com
[3] Institute of Internal Combustion Engines, Dalian University of Technology, Dalian 116024, China; pengbo.dong@dlut.edu.cn
[4] Institute for Energy Research, Jiangsu University, Zhenjiang 212013, China; y.jin@ujs.edu.cn
[5] National Key Laboratory of Marine Engine Science and Technology, Shanghai 201108, China; ppzhou2002@gmail.com (B.Z.); lysmu1@163.com (Y.L.)
* Correspondence: luohl@hrbeu.edu.cn

Abstract: This investigation employed the diffused back-illumination (DBI) technique to analyze the spray characteristics of hydrotreated vegetable oil (HVO) fuel at three injection pressures and compared them with conventional diesel fuel. The results showed that as the injection pressure increased, the peak injection rates of both the HVO and diesel increased. At injection pressures above 120 MPa, the injection rates of both fuels were nearly identical, though differences were observed at lower pressures. Increasing the injection pressure reduced the injection delay. The HVO fuel exhibited a shorter spray tip penetration, lower equivalence ratio, larger spray angle, and spray volume, but its spray angle stability was lower than that of diesel. The ambient gas entrainment rate primarily occurred in two stages, significantly influenced by the spray breakup development stage. For diesel sprays, the injection pressure mainly affected the equivalence ratio near the nozzle with minimal downstream impact. Dent's model provided better predictions of the penetration distance for diesel, while Hiroyasu's model was more accurate in predicting the penetration distance of the HVO at 120 MPa and 180 MPa. Inagaki's model performed better in predicting the spray angle for diesel, whereas Hiroyasu's model was more accurate for the HVO spray angle predictions. Through this research, a better understanding of the spray characteristics of green fuels will be achieved, providing a reference for the design and optimization of new generation engines.

Keywords: HVO fuel; diesel fuel; spray characteristics; prediction model

check for updates

Citation: Zhai, C.; Li, K.; Dong, P.; Jin, Y.; Luo, H.; Zhou, B.; Liu, Y. Experimental Study on the Spray Characteristics of Diesel and Hydrotreated Vegetable Oil (HVO) Fuels under Different Injection Pressures. *Processes* **2024**, *12*, 1697. https://doi.org/10.3390/pr12081697

Academic Editor: Albert Ratner

Received: 5 July 2024
Revised: 3 August 2024
Accepted: 13 August 2024
Published: 14 August 2024

Copyright: © 2024 by the authors. Licensee MDPI, Basel, Switzerland. This article is an open access article distributed under the terms and conditions of the Creative Commons Attribution (CC BY) license (https://creativecommons.org/licenses/by/4.0/).

1. Introduction

Compression ignition (CI) engines are widely used in vehicles, ships, and aviation [1–3]. However, as environmental awareness gradually increases, the drawbacks of traditional fossil fuels, such as unsustainability and high pollution, are becoming more apparent [4–7]. Using renewable energy can effectively reduce the environmental impact while achieving energy sustainability, and it has become a means for many countries to ensure their energy supply. For example, the European Union has set a goal for renewable energy to account for 20% of all energy use [8,9]. Hydrogenated vegetable oil (HVO) is an important component of renewable fuels, together with biodiesel, making up over four-fifths of renewable fuels used in transportation [10,11]. HVO is a sulfur-free, aromatic-free liquid mixture with a high cetane number. It is typically produced by hydrogenating vegetable oils, waste cooking oils, or animal fats [12,13].

Due to the high similarity between HVO fuel and diesel and because it is a direct drop-in fuel (which means that it can be used without modifying the power system), many researchers have conducted studies on HVOs. Zhang et al. [14] studied the macroscopic characteristics of a HVO spray through experimental and numerical methods. The results showed that the spray tip penetration grew with a decreasing tip velocity and that the cone angle increased gradually after a dramatic growth and slight drop. Combining numerical predictions with experimental studies could effectively elucidate the macroscopic characteristics of HVO spray. Cheng et al. [15] investigated the spray dynamics of HVO and diesel. Their results showed that a one-dimensional model based on Gaussian distribution and momentum conservation could effectively predict the spray characteristics. Bjørgen et al. [16] studied the combustion and soot of HVO fuel spray flames. Their results showed that diesel produced higher levels of soot compared to biodiesel and HVO, with biodiesel and HVO having similar soot levels. Khuong et al. [17] investigated the evaporation characteristics of HVO droplets under high temperature and high-pressure conditions. The results showed that HVO fuel droplets had shorter lifetimes and higher evaporation rates compared to diesel. Evaporation characteristics were influenced not only by boiling point, but also by fuel composition and thermodynamic properties such as thermal conductivity, latent heat of vaporization, and specific heat of the gas. Fajri et al. [18] used optical measurement methods to study the spray and combustion characteristics of diesel, biodiesel, and HVO under two types of heavy-duty diesel injectors. Their results showed that the injection cone angle is a parameter based on injector geometry, with cylindrical nozzles having larger cone angles and shorter liquid lengths. Bohl et al. [19] compared the spray characteristics of biofuels and conventional diesel, showing that HVO, the fuel with the lowest density among all fuels, achieved the shortest spray tip penetration and the largest cone angle, resulting in a more dispersed fuel–air mixture.

Although many researchers have conducted studies on HVO fuel, detailed investigations into its spray and mixing characteristics, particularly regarding gas entrainment and comparisons with predictive models, remain lacking. Therefore, this study systematically analyzed the spray and mixing characteristics of a HVO fuel and conventional diesel at different injection pressures for the first time, with a focus on the spray breakup and gas entrainment processes. We compared the experimental results with classical predictive models. By employing experimental methods and image processing techniques, we thoroughly explored the variations in spray volume and entrained gas mass, validating the accuracy of different predictive models. This research provides new insights for the optimization and design of fuel injection systems.

2. Experimental Conditions and Setup

Table 1 provides the detailed parameters of the injectors used in the experiment. The study utilized mini-sac injectors manufactured by Denso, characterized by a hole diameter of 0.1 mm. These injectors were of the piezoelectric type, featuring a configuration with 10 holes. Each hole had a length of 0.8 mm and an umbrella angle of 155 degrees. Additionally, the sac chamber had a radius of 0.5 mm. These specifications are illustrated in Figure 1.

Table 1. Injector parameters.

Items	Value
Injectors	Denso G4S (solenoid injector)
Type	Mini-sac
Hole number	10
Umbrella angle [°]	155
Nozzle-hole diameter (D) [mm]	0.106
Hole length [mm]	0.8
Sac radius [mm]	0.5

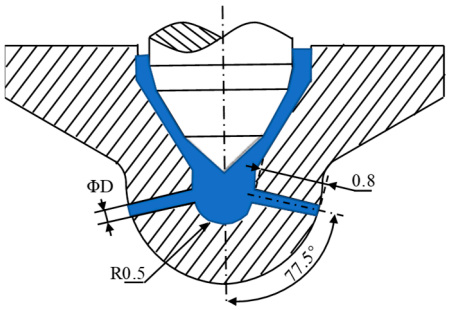


Figure 1. Schematic of 10-hole nozzles, reproduced from [20].

Tables 2 and 3 present the experimental conditions and the main properties of the fuels. The diesel sample used in this study was JIS#2 diesel, according to the Japanese Industrial Standards. The HVO fuel produced using hydrotreatment technology was primarily from waste cooking oil. At a temperature of 15 °C, their densities were 830 kg/m^3 and 779 kg/m^3, respectively. The injection mass was consistently set at 16.6 mg. The comparison was conducted using three different injection pressures ranging from 60 MPa to 180 MPa. Nitrogen was chosen as the ambient gas for the experiments. The ambient density of 16.84 kg/m^3 was used, with an ambient temperature of 300 K and an ambient pressure of 1.5 MPa.

Table 2. Experimental conditions.

Injection Condition	
Fuel	Diesel (JIS#2), HVO
Injection amount [mg]	16.6
Injection pressure (P_{inj}) [MPa]	60; 120;180
Nozzle hole diameter (D) [mm]	0.106
Ambient Condition	
Ambient gas	Nitrogen
Gas density (ρ_{amb}) [kg/m^3]	16.84
Ambient temperature [K]	300
Ambient pressure [MPa]	1.5

Table 3. Main properties of the fuel [2,21] (Reproduced with permission from author, Journal of the Energy Institute, Elsevier, 2023).

Fuel Property	Diesel (JIS#2)	HVO
Density @ 15 °C [kg/m^3]	830	779
Kin. viscosity @ 40 °C [cSt]	3.477	3.289
Distillation range [°C]	155–384	276–312
Cloud point [°C]	13	14
Derived cetane number	59.85	72.72
Lower heating value [MJ/kg]	42.9	43.81
Molecular weight [g/mol]	~203	~222
Stoichiometric air-to-fuel ratio	14.56	14.95

The injection system and observation system used in this study are shown in Figure 2. The diffuse back-illumination method (DBI) was used to obtain the spray characteristics. The light source of the observation system was provided by a high-brightness LED light source (AITEC SYSTEM Co., Ltd., Yokohama, Japan). The light from the LED source streams into the constant volume combustion chamber (CVCC) through the diffuser; after passing through the target spray, it is captured by a high-speed camera. The delay generator (DG645) simultaneously controls the ECU (electronic control unit) of the injector and the high-speed camera, ensuring that the high-speed camera can smoothly capture the

target spray. The injection pressure for the experiment was provided by a high-pressure common rail system, which can provide a stable injection pressure with a maximum pressure exceeding 300 MPa. The nitrogen cylinder was connected to the constant volume combustion chamber through a pressure reducing valve and a switch valve. The constant volume combustion chamber was connected with a pressure gauge to ensure pressure control within the chamber. Table 4 shows the optical system configurations in the DBI experiment. A visible lens (Nikon Imaging Japan Inc., Tokyo, Japa, 105 mm, f/4.8) coupled with a NAC-MEMRECAM HX-3 high-speed camera was used, providing frame rates of up to 50,000 frames per second. It should be noted that the injector was embedded above the chamber at an angle of approximately 37.5° from the horizontal direction. Therefore, the target spray was inclined at an angle of 25° with the vertical instead of vertically downward. Thus, the results of the multi-hole injectors shown in the figure were vertically scaled by multiplying by a factor of 1/cos25°.

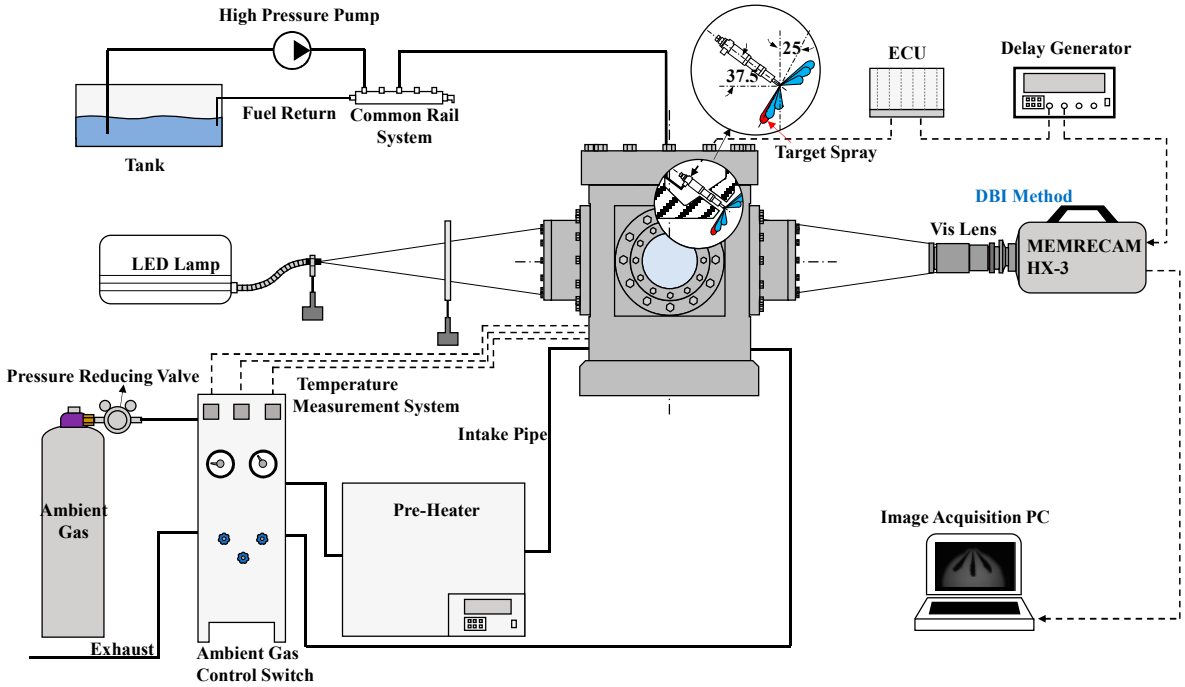


Figure 2. Experimental setup, reproduced from [20].

Table 4. Optical system configurations.

Items	Value
High-speed camera	NAC-MEMRECAM HX-3
Lens	Nikon, 105 mm
Light source	Altec LED lamp
Pulse generator	DG535
Resolution	640 × 640
Exposure [ms]	0.005
Framerate [fps]	50,000
Aperture sizes [1/f]	4.8

3. Results and Discussion

3.1. Injection Rate

The injection rate curve is crucial for understanding atomization and combustion processes. Additionally, the injection rate curve is a primary input for computational fluid dynamics (CFD) simulations. Several methods exist for measuring the fuel injection rate including the Bosch long tube method, Zeuch method, momentum flux measurement

method, etc. [19,22,23]. In this study, the injection rate curve was measured using the Bosch long-tube method. In this method, the injection rate is recorded by measuring the pressure wave that is produced by an injector when it is injected into a length of compressible fluid. Hwang et al. discussed the Bosch long-tube method and theory; detailed information can be found in this paper [24]. Figure 3 shows the injection rate curves for different fuels at injection pressures of 60 MPa, 120 MPa, and 180 MPa. The injection mass for each injection pressure was set to the same 16.6 mg. It can be observed that as the injection pressure increased, the peak of the injection rate became higher. This is because the injection rate is primarily controlled by the effective flow area and fuel momentum. It is noteworthy that by comparing the injection rates of different fuels, it can be seen that under conditions of 120 MPa and 180 MPa, the injection rates of the two fuels were almost identical.

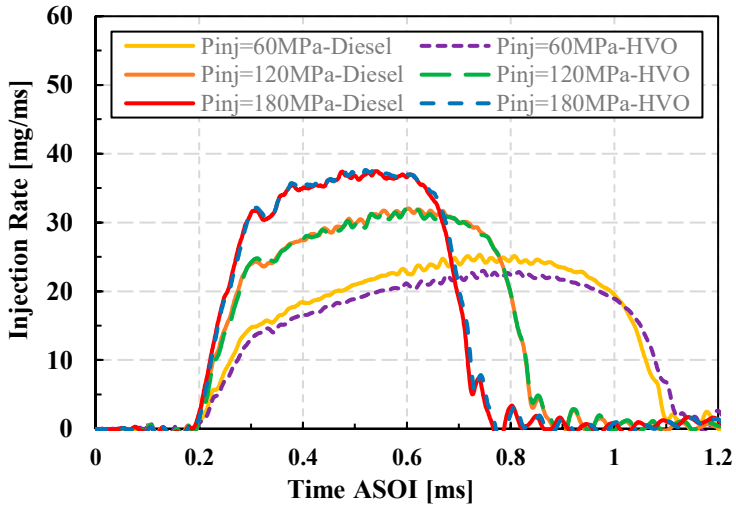


Figure 3. Injection rate.

However, at an injection pressure of 60 MPa, the injection rates of the two fuels were different. This may be due to differences in the physical properties of the fuels (density and viscosity, etc.) leading to different initial pressure buildups in the sac chamber under low injection pressure conditions, which in turn caused changes in the needle valve movement characteristics (lift height and lift speed, etc.).

3.2. Macroscopic Characteristics of the Spray

Figure 4 shows the original spray image obtained using the DBI method. It can be seen that the injection delay decreased with increasing pressure. This is because higher injection pressure results in a faster pressure buildup in the sac chamber, leading to a quicker needle valve lift, thus shortening the injection delay. Additionally, it can be seen that at the same injection pressure, the injection delays of different fuels were similar. Although the physical properties of different fuels may lead to differences in injection delay, a detailed analysis of the injection delay was not possible in this study due to the limitation of the frame rate (FPS). In future research, a microscopic observation method can be used to analyze the injection delays of different fuels in detail. Furthermore, it can be seen that as the pressure increased, the turbulence intensity at the spray head became stronger, and clear turbulent vortices appeared at the boundary of the spray head. Compared to diesel, HVO has a wider spray width, which can be attributed to its lower viscosity and lower surface tension. This will result in a higher Weber number and promote secondary fragmentation of the fuel.

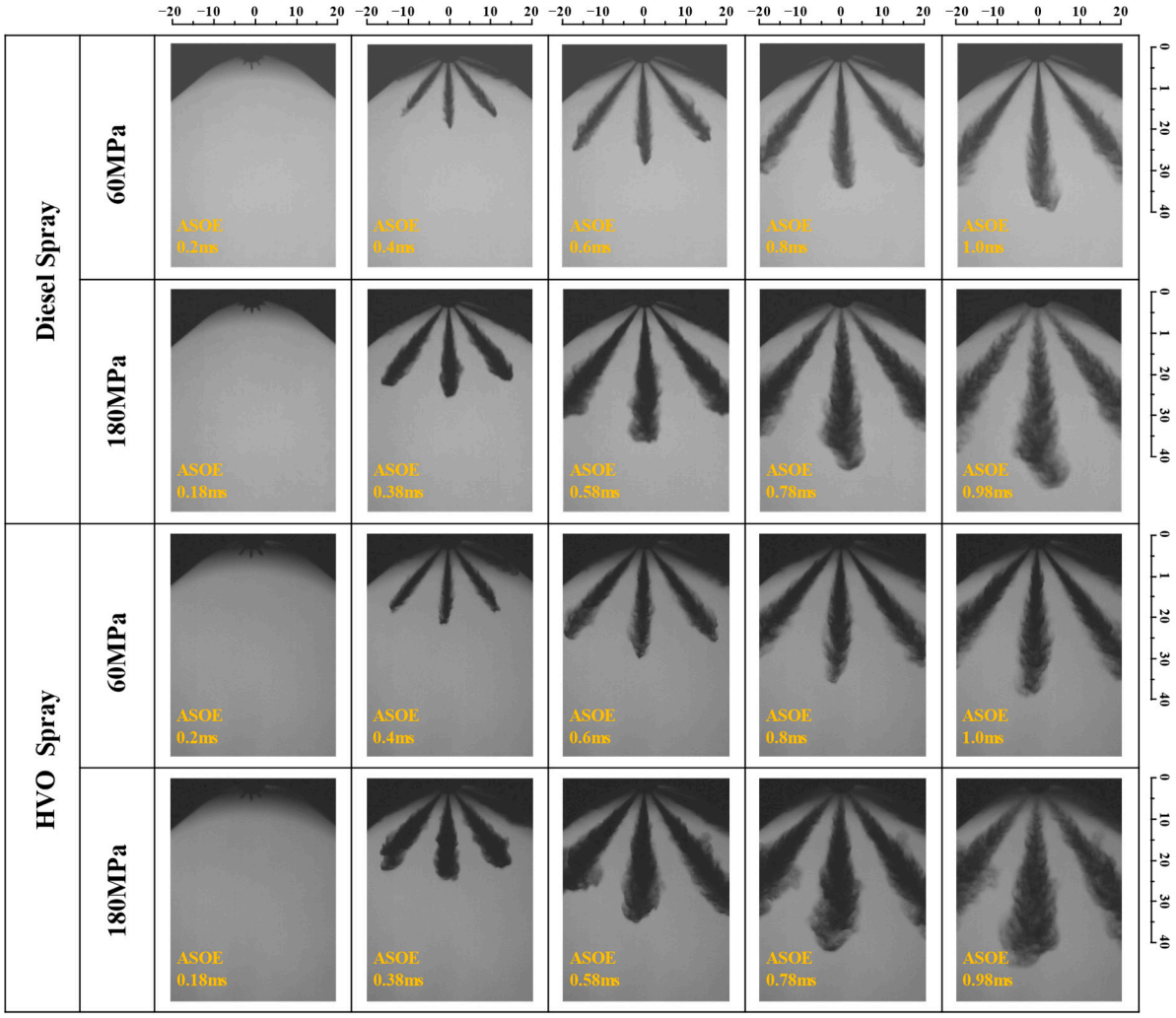


Figure 4. Diffuse back-illumination images of the spray.

After the above analysis, we mainly used the non-evaporative spray images obtained by the DBI method to study the spray characteristics. However, relying solely on non-evaporative spray images may not provide a comprehensive understanding of the details. To overcome this limitation, we processed the non-evaporative spray images using MATLAB R2021a software. The specific image processing steps and definitions are shown in Figure 5. First, we subtracted the target spray image (Figure 5b) from the background image (Figure 5a). Next, the resulting image was binarized. For the binarization process, we selected 15% of the maximum image value as the threshold [25,26]. The binarized image is shown in Figure 5c. Finally, the binarized image was used to define the macroscopic characteristics of the spray. In this case, the distance between the nozzle tip and the spray tip was selected to define the spray tip penetration. The angle at half the spray tip penetration is defined as the spray angle. Using this definition, we obtained more detailed macroscopic spray characteristics, as shown in Figure 5c.

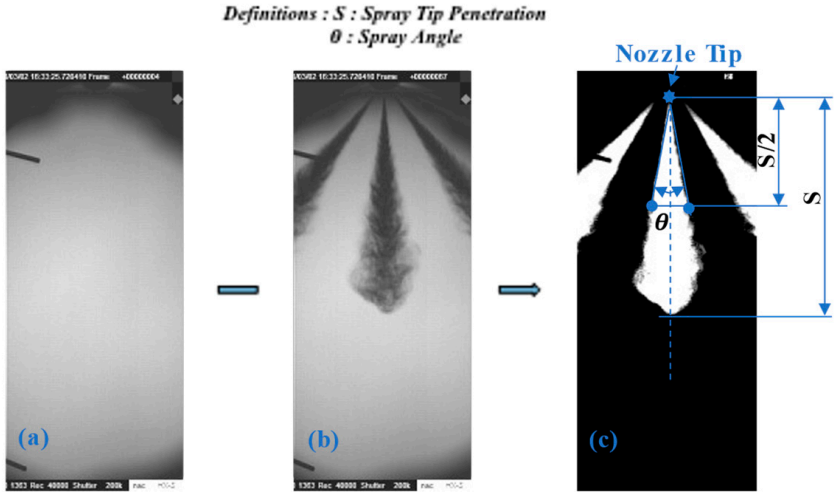


Figure 5. Definition of spray properties [26] (Reproduced with permission from author, Fuel, Elsevier, 2021).

3.2.1. Spray Tip Penetration, Spray Angle and Spray Area

Figure 6 shows the variation in the macroscopic spray tip penetration of two fuels under different injection pressures. From the figure, it can be seen that the spray tip penetration increased with the rise in injection pressure. However, as the injection pressure increased from 120 MPa to 180 MPa, the effect of injection pressure on the spray tip penetration significantly decreased. Comparing the spray tip penetration of different fuels, it can be seen that at the same time, the HVO fuel had a shorter spray tip penetration. This is because HVO fuel has a higher Weber number, which promotes fuel atomization. The fragmented fuel has a larger radial velocity, reducing the axial velocity of the spray and thereby shortening the spray tip penetration. It is worth noting that in the initial stage of the spray, the HVO fuel had a greater spray tip penetration distance, which may be attributed to the low viscosity characteristics of the HVO affecting the internal flow of the nozzle. Additionally, in the early stage of injection, when the spray was not fully fragmented, the lower density of HVO resulted in a larger volumetric flow rate under the same mass flow rate.

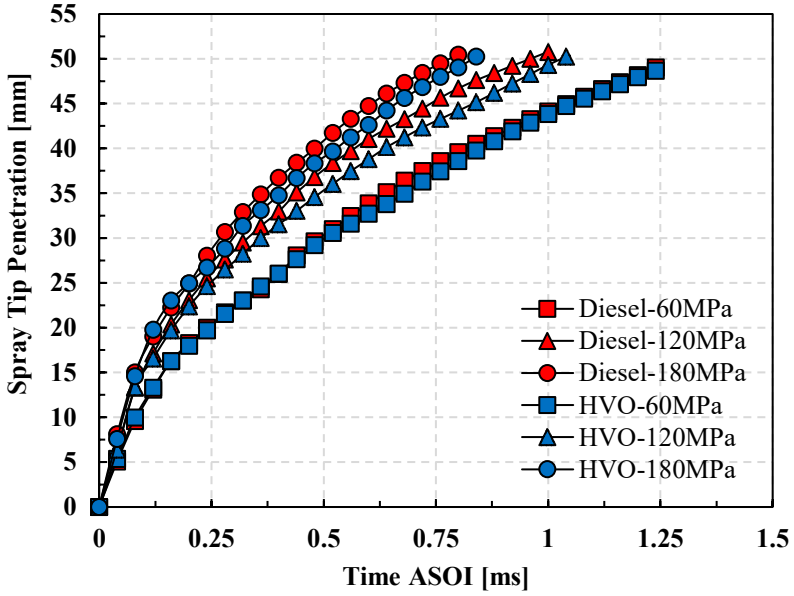


Figure 6. Spray tip penetration with different conditions.

Figure 7 shows the spray angle variation characteristics of the two fuels at different injection pressures. From the figure, we can see that as the injection pressure increased, the spray angle of the fuel gradually increased. This is because the increase in injection pressure enhances the center axial velocity of the spray. The fully fragmented spray can be assumed to be a gas jet, and the radial distribution of the spray velocity satisfies the following equation [20,27,28].

$$v = v_m \left[1 - \left(\frac{r}{R}\right)^{1.5}\right]^2 \quad (1)$$

where r is the radius position of any spray cross section, R is the maximum radius of the cross-section, v is the velocity of the spray cross section where the radius is r, and v_m is the velocity at the center axis of the spray cross section.

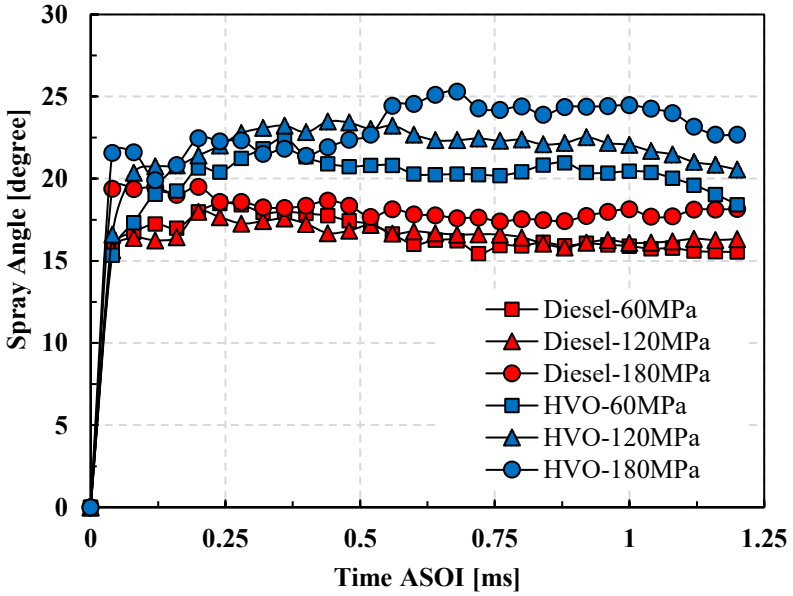


Figure 7. Spray angle with different conditions.

From this, it can be seen that a larger central axial velocity implies a greater radial velocity. Additionally, it can be observed that compared to diesel fuel, the HVO fuel was more susceptible to the influence of injection pressure, resulting in an increased spray angle. As mentioned earlier, HVO fuel has a lower surface tension and viscosity, which makes it easier to atomize than diesel fuel and is more affected by injection pressure. It is also worth noting that although the HVO spray has a larger spray angle, it seems to become more unstable compared to diesel fuel, especially the spray angle of HVO fuel under 180 MPa conditions. From the figure, we can also see that as the injection pressure increased, the time for the spray angle to stabilize gradually shortened, because a higher injection pressure reduces the breakup time of the spray. To compare the changes in the spray angle more concisely and clearly, we averaged the spray angle during the stable period. The averaging period was selected from ASOI 0.5 ms to 1 ms. The average results are shown in Figure 8. It can be seen more clearly from the figure that the average spray angle of HVO fuel was significantly larger than that of diesel fuel. As the injection pressure increased, the average spray angle of both fuels gradually increased, with HVO fuel showing a more pronounced change. At 60 MPa, the ratio of the average spray angle of HVO fuel to diesel fuel was about 1.34. As the injection pressure increased, this ratio gradually rose and was about 1.36 at 120 MPa and 1.4 at 180 MPa injection conditions. This indicates that the injection pressure has a greater impact on the HVO spray. It also shows that the change in fuel properties does not have a linear proportional effect on the spray angle.

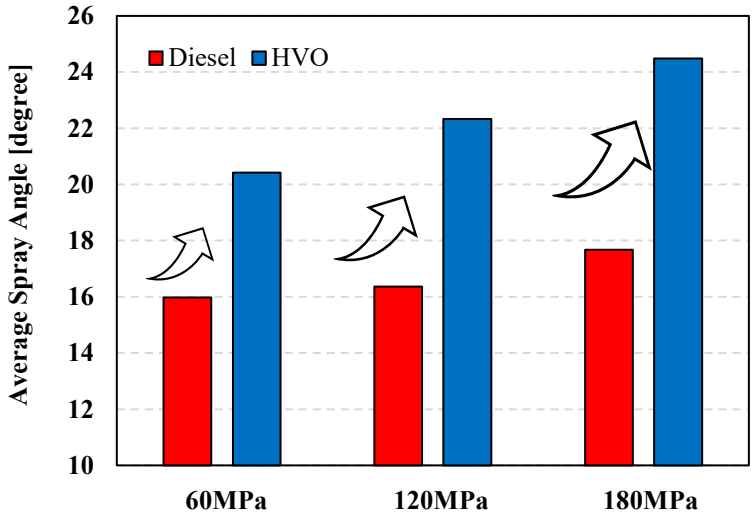


Figure 8. Average spray angle with different conditions.

The spray area can indirectly indicate the mixing of fuel and gas [29,30]. Figure 9 shows the variation in the spray areas for the two types of fuel over time. It can be seen that at the same spray tip penetration, the spray area increased with rising injection pressure. However, as the injection pressure continued to rise, this difference gradually decreased. This phenomenon slightly differs from the conclusion proposed by Delacourt et al. The reason for this discrepancy may be due to the structure of the injector and the lower injection pressure [29]. At a specified spray tip penetration, the spray area is related to the spray angle. In diesel sprays, due to higher viscosity, the effect of injection pressure on the spray angle is relatively small (compared to the hole diameter and ambient density). During the calculation of the spray area, the influence of the spray angle is further weakened, leading to the conclusion that the spray area is independent of the injection pressure given the spray tip penetration. However, in previous research with higher pressures, and due to the influence of the injector's structure and fuel properties, the HVO fuel showed a significantly different spray area at low injection pressures. Comparing the spray areas of different fuels at the same injection pressure, the spray area of HVO was significantly larger than that of diesel, which also means that the HVO spray entrains more air, resulting in better mixing.

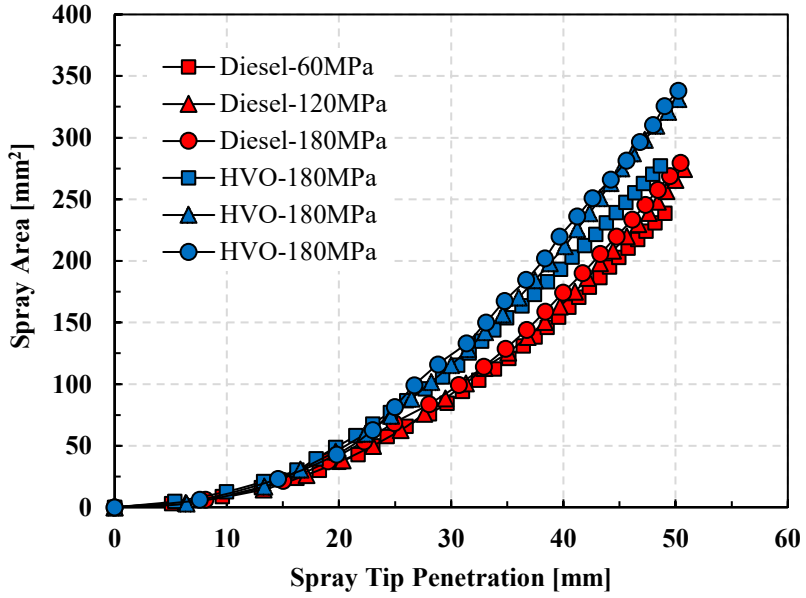


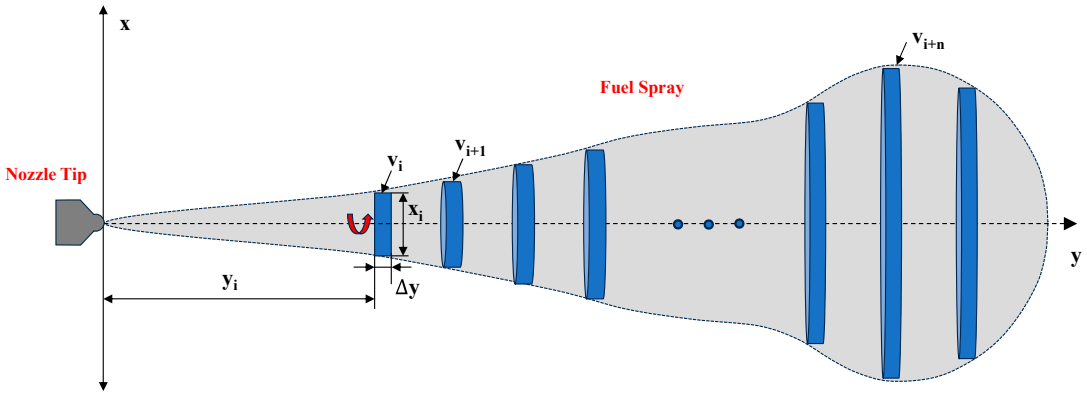
Figure 9. Spray area with different conditions.

3.2.2. Spray Volume and Entrainment

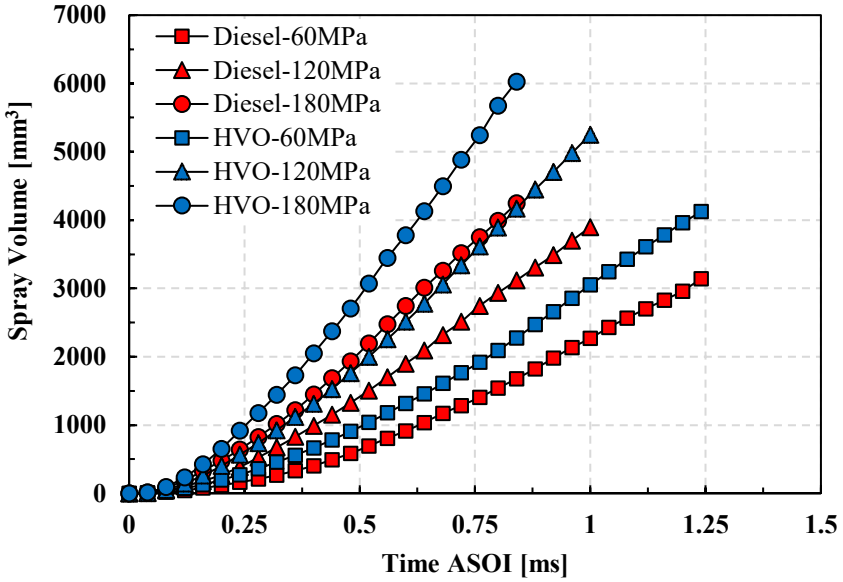
The entrainment process of fuel directly affects its combustion and emissions. Therefore, analyzing the entrainment process is essential. In our previous research, we proposed a spray volume calculation method based on image processing [26]. The calculation principle of spray volume is shown in Figure 10a, and mainly involves binarizing the spray image, extracting the radial diameter x_i of the spray, performing rotational processing to calculate the unit radial volume, and finally accumulating these to obtain the entire spray volume v.

$$v = \sum_{i=1}^{y} v_i = \sum_{i=1}^{y} \pi \left(\frac{x_i}{2}\right)^2 \Delta y \quad (2)$$

where i is the number of pixels in the image, y is the total length of the spray, v_i is the unit radial volume, and Δy is the pixel length of each row.



(**a**) The calculation principle of spray volume



(**b**) Spray volume with different conditions

Figure 10. Spray volume calculation method and results [26] (Reproduced with permission from author, Fuel, Elsevier, 2021).

By obtaining the spray volume, we can calculate the mass of entrained air.

$$M_{gas} = v_{gas}\rho_{gas} = \left(v - v_{fuel}\right)\rho_{gas} \quad (3)$$

where M_{gas} is the mass of the entrained gas, v_{gas} is the volume of the entrained gas, v_{fuel} is the volume of the fuel (calculated from the injection rate), and ρ_{gas} is the density of the ambient gas.

By using the mass of the entrained air, the mass flow rate of the entrained gas can be calculated.

$$\dot{M}_g = \frac{M_{gas}(t) - M_{gas}(t - \Delta t)}{\Delta t} \tag{4}$$

where $\dot{M}_g$ is the mass flow rate of the entrained gas, and Δt is the time interval (here taken as 0.02 ms). For specific definitions of spray volume and entrainment, please refer to our previously published article [26]. These details will not be reiterated here.

Figure 10 shows the spray volume and entrained air mass calculated using Equations (2) and (3). As shown in the figure, consistent with the results of the spray area, the spray volume and the entrained air mass increased with rising injection pressure. Under the same injection pressure, the spray angle of HVO fuel was larger, leading to a greater spray volume and entrained air mass. This helps achieve more complete combustion of the fuel, promotes soot oxidation, and reduces soot formation. Additionally, increasing the injection pressure from 60 MPa to 120 MPa resulted in more significant changes in the spray volume and entrained air mass compared to increasing the injection pressure from 120 MPa to 180 MPa. This indicates that as the injection pressure increases, the effect of injection pressure on the spray volume and entrained air mass diminishes.

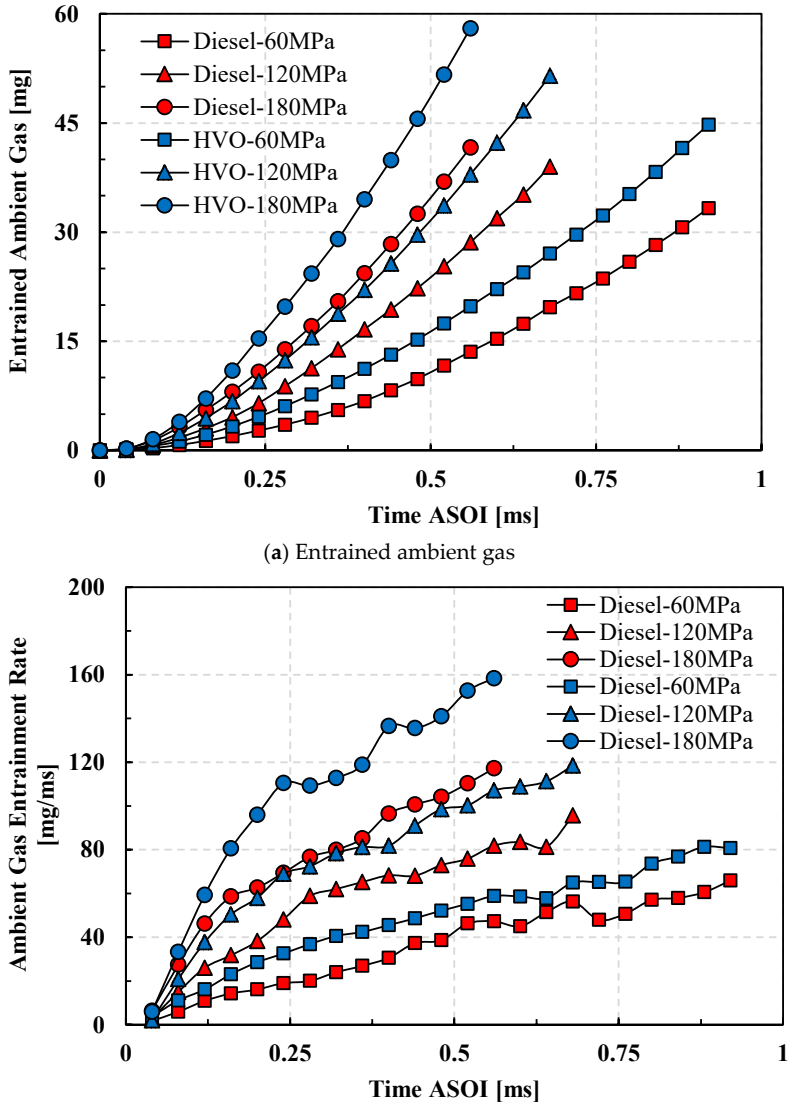
Figure 11a shows the rate of change of the ambient entrained air mass calculated by Equation (4). From the figure, it can be observed that the rate of ambient entrained air mass change has two stages: a continuous increase stage and a periodic variation stage. At the beginning of injection, the rate of ambient entrained air is relatively low but shows a rapid increase. As injection continues, the entrained air rate enters a phase of periodic growth. This is because at the initial stage of injection, due to the high injection velocity, there is significant variation in the spray tip penetration and the spray angle is not stable, remaining relatively small. Simultaneously, the spray has not completely broken up, and the entrainment process is still developing. With the stabilization of secondary spray broken up, the entrained air rate gradually stabilizes, leading to periodic variations in the entrainment of the spray.

By calculating the entrained air mass, we can determine the average equivalence ratio of the spray, as shown by the following formula:

$$\varphi_{avg} = \frac{M_{fuel}/M_{gas}}{\left(m_{fuel}/m_{gas}\right)_{st}} \tag{5}$$

where M_{fuel} is the injected fuel mass, M_{gas} is the entrained air mass, and $\left(m_{fuel}/m_{gas}\right)_{st}$ is the stoichiometric equivalence ratio for diesel, taken as 14.7 in this paper.

Figure 12 shows the results of calculating the average equivalence ratio of the spray. It can be observed that increasing the injection pressure reduced the average equivalence ratio of the spray. In terms of trends, the pressure primarily affect was in reducing the equivalence ratio of diesel spray near the nozzle, with a smaller impact downstream. This indicates that increased pressure mainly affects the primary broken up diesel spray, with a lesser effect on secondary fragmentation. Compared to diesel, HVO showed a lower average equivalence ratio. Although increasing pressure decreased the average equivalence ratio of the HVO spray, the effect of increasing pressure on the HVO spray was less significant compared to diesel. From the trend in the average equivalence ratio of the HVO spray, increasing pressure had little impact on the upstream and downstream average equivalence ratio of the spray.



(**a**) Entrained ambient gas

(**b**) Ambient gas entrainment rate

Figure 11. Characteristics of entrainment with different conditions.

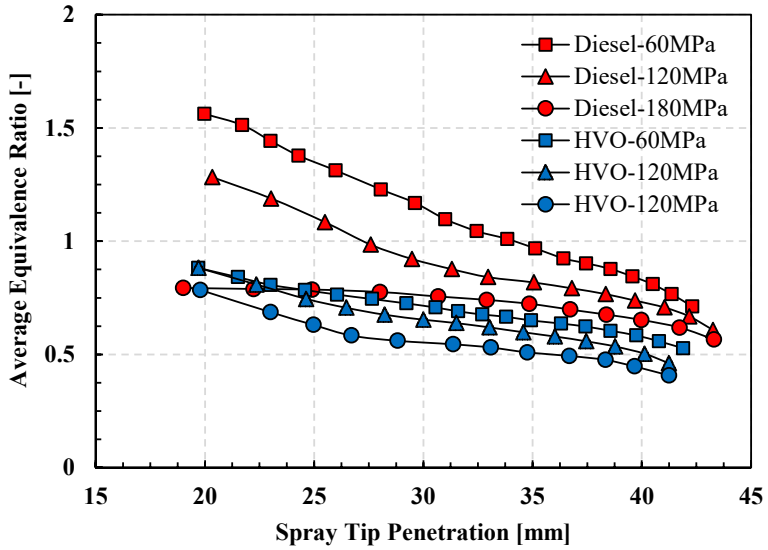


Figure 12. Average equivalence ratio.

3.3. Empirical Prediction

3.3.1. Spray Tip Penetration Prediction

Predicting the spray characteristics effectively reduces the engine design costs. Parameters such as spray tip penetration and spray angle have long been of interest to researchers. To assess the predictive accuracy of existing spray models for HVO sprays, we conducted comparative analyses between different prediction models and the experimental data. Regarding spray tip penetration prediction models, many researchers have focused on them, and Dent et al. proposed a widely used model known for its simplicity and effectiveness in prediction [31].

$$S = 0.37\left(\frac{\Delta P}{\rho_{gas}}\right)^{0.25}\left(\frac{294}{T_{gas}}\right)^{0.5}(Dt)^{0.5} \tag{6}$$

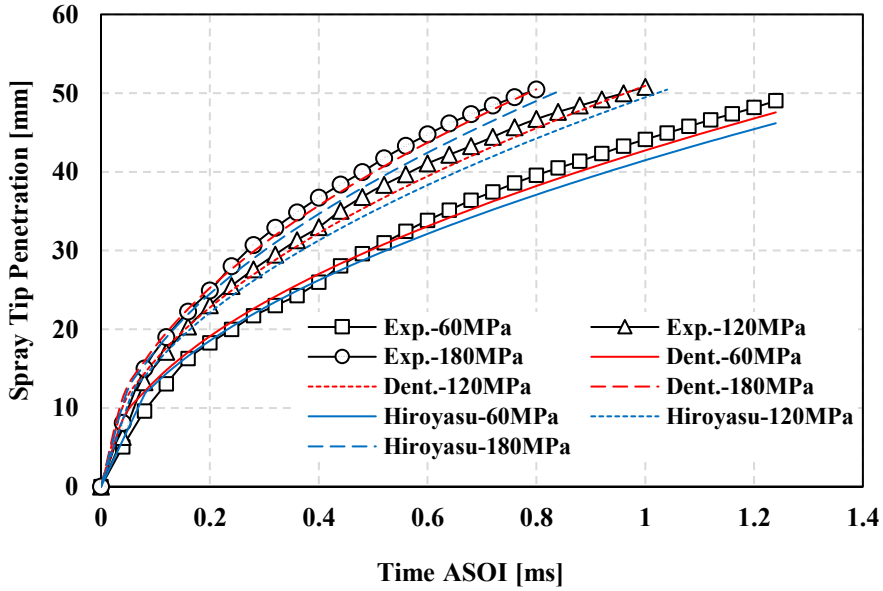
where S is the spray tip penetration of the spray, ΔP is the difference between the injection pressure and ambient pressure, ρ_{gas} is the density of the ambient gas, D is the diameter of the nozzle hole, and t is time.

Hiroyasu et al. developed a spray tip penetration model that divides the spray tip penetration into two stages and establishes different models for each stage [32].

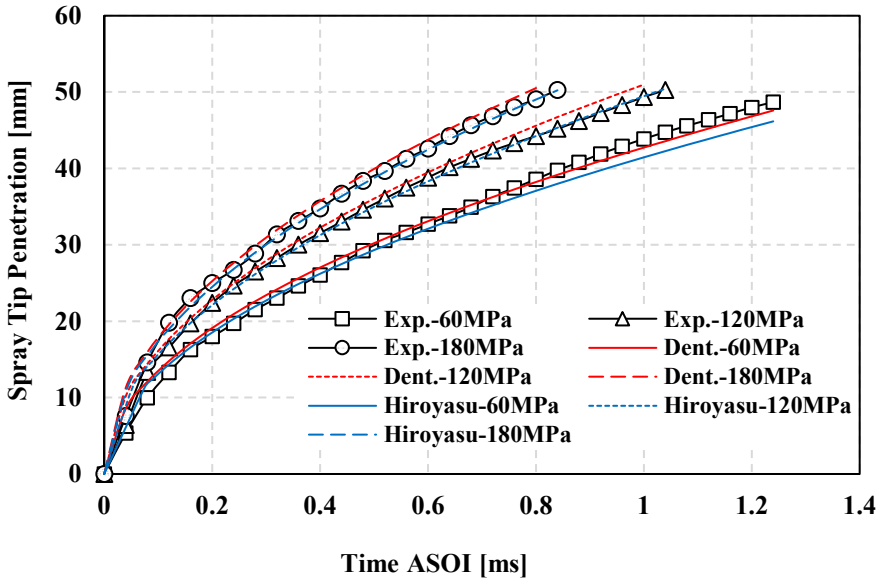
$$\begin{aligned} S &= 0.39\left(\tfrac{2\Delta P}{\rho_{fuel}}\right)^{0.5} t \qquad t < t_b \\ S &= 2.95\left(\tfrac{\Delta P}{\rho_{gas}}\right)^{0.25}(Dt)^{0.5} \qquad t_b \geq t \\ t_b &= 28.65\frac{D\rho_{fuel}}{\sqrt{\Delta P \rho_{gas}}} \end{aligned} \tag{7}$$

where ρ_{fuel} is the density of the fuel, and t_b is the breakup time.

Figure 13 compares the experimental data with the spray tip penetration prediction models. The black line represents the experimental data, the red line shows the predictions from Dent's model, and the blue line shows predictions from Hiroyasu's model. For the diesel spray predictions, Dent's model performed well in predicting the data at the end of injection under different injection pressures, while Hiroyasu's model slightly underestimated the spray tip penetration. For the HVO sprays, at the end of injection, Hiroyasu's model predicted the penetration distance better at 120 MPa and 180 MPa, while Dent's model overestimated the spray tip penetration. At 60 MPa, Dent's model predicted reasonably well, whereas Hiroyasu's model slightly underestimated the spray tip penetration. One point of note is that for all conditions, there was a difference at the initial stage of injection prediction by the 0-D model. This difference may be attributed to the definition of the start of injection (SOI). In this study, this was defined as the frame before the first spray image, resulting in some error in determining the SOI accurately due to limitations in frames per second of the camera. This poses a challenge for refining prediction models. Of course, the influence of model parameters is crucial; different nozzle types directly affect the internal flow conditions, thereby influencing variations in the prediction model parameters. Therefore, more accurate prediction models should fully consider the characteristics of the internal nozzle flow (e.g., cavitation number, length-to-diameter ratio, Reynolds number, turbulence intensity, etc.).



(**a**) Comparison of diesel spray and prediction model



(**b**) Comparison of HVO spray and prediction models

Figure 13. Comparison of the experimental data of the spray tip penetration with the prediction models.

3.3.2. Spray Angle Prediction

Similarly to the spray tip penetration, many researchers have also studied prediction models for spray angles. Hiroyasu et al. proposed the following spray angle prediction model [33].

$$\theta_{\frac{S}{2}} = 0.413\left(\frac{\rho_{gas}\Delta P D^2}{\mu_{gas}^2}\right)^{0.25} \tag{8}$$

where $\theta_{\frac{S}{2}}$ represents the spray angle, and μ_{gas} is the dynamic viscosity of the gas.

Inagaki et al. used multiple linear regression analysis to obtain the spray angle prediction model [34].

$$\theta_{\frac{S}{2}} = c\left(\frac{\rho_{gas}}{\mu_{gas}^2}\right)^{0.25} P_{inj}^{0.18}\left(\frac{L}{D}\right)^{-0.14} \tag{9}$$

where c is the model constant, and L is the length of the orifice.

In addition, Kitaguchi et al. proposed the following spray angle prediction model [35].

$$\theta_{\frac{S}{2}} = 26\Delta P^{-0.02}\rho_{gas}^{0.385}D^{0.15} \quad (10)$$

Figure 14 illustrates the comparison between three different spray angle prediction models and experimental data. The constant c in the Inagaki model is 0.00152 [26]. From the figure, it is evident that compared to the diesel spray, Hiroyasu's model overestimated the spray angle, while the Inagaki and Kitaguchi models underestimated the spray angle. Overall, the Inagaki model performed relatively well in predicting the diesel experimental results. For HVO sprays, all models underestimated the spray angle, with the Hiroyasu model relatively better at predicting the experimental results compared to the other spray angle prediction models.

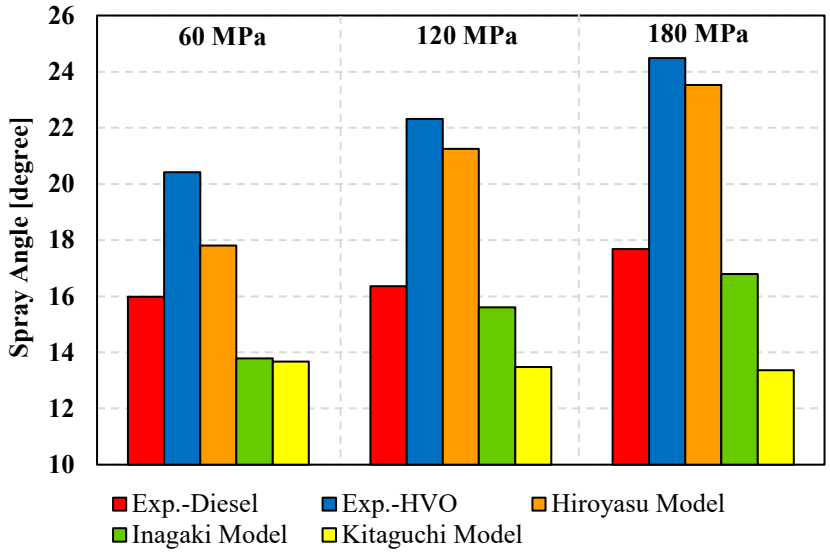


Figure 14. Comparison of the experimental data of the spray angle with the prediction models.

4. Conclusions

In this study, the spray characteristics of the HVO fuel were analyzed using DBI technology, and the differences compared to conventional diesel were identified. The specific conclusions are as follows:

(1) As the pressure increased, the peak injection rate also increased. At injection pressures above 120 MPa, the injection rates of both fuels were nearly identical. However, under low-pressure conditions, the injection rates differed, which may be due to the influence of fuel properties on the initial sac pressure establishment and needle valve movement trajectory.

(2) Increased pressure shortened the injection delay. Although different fuel properties may affect injection delay, further detailed analysis is required. Compared to diesel, the HVO spray showed a wider spray width, attributed to its lower viscosity and surface tension.

(3) Increased injection pressure enhanced the spray tip penetration and spray angle, but as the injection pressure continued to increase, its effect on the spray tip penetration diminished. Compared to diesel, HVO fuel had a shorter spray tip penetration, larger spray angle, and area, but its spray angle stability was lower than that of diesel. In the initial stage, the HVO fuel exhibited a larger spray tip penetration, which may be due to incomplete fuel breakup and its low viscosity. It is worth noting that the effect of increased injection pressure on spray area differed from that in previous studies, possibly due to the injector structure and lower injection pressure.

(4) Increasing injection pressure raised the spray volume and entrained air mass, reducing the average equivalence ratio of the spray. As the injection pressure increased, its influence on spray volume and entrained air mass decreased. The HVO fuel had a larger spray volume, higher entrained air mass, and lower average equivalence ratio. The ambient gas entrainment rate mainly occurred in two stages, primarily influenced by the spray breakup development stage. For the diesel spray, the injection pressure mainly affected the equivalence ratio near the nozzle, with relatively minor effects downstream. The change in the equivalence ratio of the HVO spray showed that the effect of the increased pressure on both the upstream and downstream regions was relatively small.

(5) For the diesel spray tip penetration, Dent's model performed well in predicting data at the end of injection under different injection pressures. For the HVO spray tip penetration, Hiroyasu's model better predicted the spray tip penetration at 120 MPa and 180 MPa, while Dent's model performed better at 60 MPa. It is important to note that both models showed differences in predictions during the initial stage of injection, which may be attributed to the definition of start of injection (SOI) and the accuracy of the model parameters. For the diesel spray angle, the Inagaki model performed relatively well, while for the HVO spray angle, the Hiroyasu model performed better.

In this study, we conducted a detailed analysis of the spray characteristics of HVO and performed a quantitative analysis of its entrainment characteristics. We were the first to perform a comprehensive analysis of predictive models for HVO spray characteristics, highlighting the limitations of existing models. Additionally, the results indicate that HVO sprays exhibit completely different characteristics compared to diesel sprays, especially under low-pressure injection. Under the same conditions, the HVO spray has a larger spray angle, shorter spray penetration, and greater entrainment, all of which will impact the injection strategies in an actual engine to achieve the appropriate spatial equivalence ratio and fuel distribution. Additionally, common spray predictive models lack fuel properties as input parameters, highlighting the need for more concise predictive equations that include fuel property parameters to accommodate different fuels.

Author Contributions: Conceptualization, C.Z. and H.L.; Methodology, C.Z. and H.L.; Validation, H.L.; Formal analysis, C.Z.; Investigation, C.Z. and H.L.; Resources, K.L., B.Z., Y.L. and P.D.; Data curation, C.Z.; Writing—original draft preparation, C.Z.; Writing—review and editing, H.L., K.L., P.D. and Y.J.; Visualization, C.Z.; Supervision, H.L., B.Z. and Y.L. All authors have read and agreed to the published version of the manuscript.

Funding: This study was financially supported by the Open Research Subject of Key Laboratory of Fluid Machinery and Engineering (Xihua University), Sichuan Province (LTJX-2024 002), the National Key Laboratory of Marine Engine Science and Technology (LAB-2023-01), the Open Fund of Key Laboratory of Oil & Gas Equipment, Ministry of Education (Southwest Petroleum University) (OGE202302-04), the Fundamental Research Funds for the Central Universities (3072023CFJ0304), and the Funded by Shandong Postdoctoral Science Foundation (SDCX-ZG-202400247).

Data Availability Statement: The original contributions presented in the study are included in the article, further inquiries can be directed to the corresponding author.

Acknowledgments: The authors would like to acknowledge the Mazda Motor Corporation for their support of the equipment apparatus.

Conflicts of Interest: The authors declare no conflicts of interest.

References

1. Zhen, X.; Wang, Y.; Liu, D. Bio-butanol as a new generation of clean alternative fuel for SI (spark ignition) and CI (compression ignition) engines. *Renew. Energy* **2020**, *147*, 2494–2521. [CrossRef]
2. Luo, H.; Jin, Y.; Zhai, C.; Chang, F.; Xing, W.; Nishida, K.; Ogata, Y. Very low soot formation with modulated liquid length and lift-off length of diesel spray flame. *J. Energy Inst.* **2023**, *111*, 101383. [CrossRef]

3. Zhai, C.; Zhang, G.; Jin, Y.; Nishida, K.; Ogata, Y.; Luo, H. Characterization of diesel spray combustion using two-color pyrometry and OH∗ chemiluminescence imaging-comparison between micro-hole and ultra-high injection pressure effects. *J. Energy Inst.* **2022**, *103*, 104–116. [CrossRef]
4. Abbasi, T.; Abbasi, S. Is the use of renewable energy sources an answer to the problems of global warming and pollution? *Crit. Rev. Environ. Sci. Technol.* **2012**, *42*, 99–154. [CrossRef]
5. Armaroli, N.; Balzani, V. The future of energy supply: Challenges and opportunities. *Angew. Chem. Int. Ed.* **2007**, *46*, 52–66. [CrossRef] [PubMed]
6. Zhai, C.; Liu, E.; Zhang, G.; Xing, W.; Chang, F.; Jin, Y.; Luo, H.; Nishida, K.; Ogata, Y. Similarity and normalization study of fuel spray and combustion under ultra-high injection pressure and micro-hole diameter conditions–spray characteristics. *Energy* **2024**, *288*, 129684. [CrossRef]
7. Eremeeva, A.M.; Ilyushin, Y.V. Automation of the control system for drying grain crops of the technological process for obtaining biodiesel fuels. *Sci. Rep.* **2023**, *13*, 14956. [CrossRef] [PubMed]
8. Scarlat, N.; Dallemand, J.-F.; Monforti-Ferrario, F.; Banja, M.; Motola, V. Renewable energy policy framework and bioenergy contribution in the European Union–An overview from National Renewable Energy Action Plans and Progress Reports. *Renew. Sustain. Energy Rev.* **2015**, *51*, 969–985. [CrossRef]
9. Musiał, W.; Zioło, M.; Luty, L.; Musiał, K. Energy policy of European Union member states in the context of renewable energy sources development. *Energies* **2021**, *14*, 2864. [CrossRef]
10. Suarez-Bertoa, R.; Kousoulidou, M.; Clairotte, M.; Giechaskiel, B.; Nuottimäki, J.; Sarjovaara, T.; Lonza, L. Impact of HVO blends on modern diesel passenger cars emissions during real world operation. *Fuel* **2019**, *235*, 1427–1435. [CrossRef]
11. Eremeeva, A.M.; Kondrasheva, N.K.; Khasanov, A.F.; Oleynik, I.L. Environmentally friendly diesel fuel obtained from vegetable raw materials and hydrocarbon crude. *Energies* **2023**, *16*, 2121. [CrossRef]
12. Zeman, P.; Hönig, V.; Kotek, M.; Táborský, J.; Obergruber, M.; Mařík, J.; Hartová, V.; Pechout, M. Hydrotreated vegetable oil as a fuel from waste materials. *Catalysts* **2019**, *9*, 337. [CrossRef]
13. Millo, F.; Bensaid, S.; Fino, D.; Marcano, S.J.C.; Vlachos, T.; Debnath, B.K. Influence on the performance and emissions of an automotive Euro 5 diesel engine fueled with F30 from Farnesane. *Fuel* **2014**, *138*, 134–142. [CrossRef]
14. Zhang, Z.; Lu, Y.; Ren, H.; Roskilly, A.P.; Chen, L.; Smallbone, A.; Wang, Y. Experimental and numerical investigation on the macroscopic characteristics of hydrotreated vegetable oil (HVO) spray. *Energy Procedia* **2017**, *142*, 474–480. [CrossRef]
15. Cheng, Q.; Tuomo, H.; Kaario, O.T.; Martti, L. Spray dynamics of HVO and EN590 diesel fuels. *Fuel* **2019**, *245*, 198–211. [CrossRef]
16. Bjørgen, K.O.P.; Emberson, D.R.; Løvås, T. Combustion and soot characteristics of hydrotreated vegetable oil compression-ignited spray flames. *Fuel* **2020**, *266*, 116942. [CrossRef]
17. Khuong, L.S.; Hashimoto, N.; Konno, Y.; Suganuma, Y.; Nomura, H.; Fujita, O. Droplet evaporation characteristics of hydrotreated vegetable oil (HVO) under high temperature and pressure conditions. *Fuel* **2024**, *368*, 131604. [CrossRef]
18. Fajri, H.; Rieß, S.; Mallada, R.C.; Ruoff, I.; Wensing, M. Optical measurements of two cylindrical and conical heavy-duty diesel injector nozzels–A comparison of reference diesel, HVO, and RME fuels. *Energy Convers. Manag.* **2023**, *285*, 117018. [CrossRef]
19. Bohl, T.; Tian, G.; Smallbone, A.; Roskilly, A.P. Macroscopic spray characteristics of next-generation bio-derived diesel fuels in comparison to mineral diesel. *Appl. Energy* **2017**, *186*, 562–573. [CrossRef]
20. Zhai, C.; Chang, F.; Jin, Y.; Luo, H. Investigations on the Diesel Spray Characteristic and Tip Penetration Model of Multi-Hole Injector with Micro-Hole under Ultra-High Injection Pressure. *Sustainability* **2023**, *15*, 11114. [CrossRef]
21. Fathurrahman, N.A.; Ginanjar, K.; Devitasari, R.D.; Maslahat, M.; Anggarani, R.; Aisyah, L.; Soemanto, A.; Solikhah, M.D.; Thahar, A.; Wibowo, E. Long-term storage stability of incorporated hydrotreated vegetable oil (HVO) in biodiesel-diesel blends at highland and coastal areas. *Fuel Commun.* **2024**, *18*, 100107. [CrossRef]
22. Arcoumanis, C.; Baniasad, M.; Banias, M. Analysis of consecutive fuel injection rate signals obtained by the Zeuch and Bosch methods. *SAE Trans.* **1993**, *102*, 1371–1384.
23. Luo, F.; Cui, H.; Dong, S. Transient measuring method for injection rate of each nozzle hole based on spray momentum flux. *Fuel* **2014**, *125*, 20–29. [CrossRef]
24. Hwang, J.; Bae, C.; Gupta, T. Application of waste cooking oil (WCO) biodiesel in a compression ignition engine. *Fuel* **2016**, *176*, 20–31. [CrossRef]
25. Jin, Y.; Dong, P.; Zhai, C.; Nishida, K.; Ogata, Y.; Leng, X. Internal flow and spray characterization of multi-hole injectors: Comparison with single-hole injectors. *Energy Fuels* **2020**, *34*, 7490–7501. [CrossRef]
26. Zhai, C.; Jin, Y.; Nishida, K.; Ogata, Y. Diesel spray and combustion of multi-hole injectors with micro-hole under ultra-high injection pressure–non-evaporating spray characteristics. *Fuel* **2021**, *283*, 119322. [CrossRef]
27. Desantes, J.M.; Payri, R.; Salvador, F.J.; Gil, A. Development and validation of a theoretical model for diesel spray penetration. *Fuel* **2006**, *85*, 910–917. [CrossRef]
28. Desantes, J.M.; Pastor, J.V.; García-Oliver, J.M.; Briceño, F.J. An experimental analysis on the evolution of the transient tip penetration in reacting Diesel sprays. *Combust. Flame* **2014**, *161*, 2137–2150. [CrossRef]
29. Delacourt, E.; Desmet, B.; Besson, B. Characterisation of very high pressure diesel sprays using digital imaging techniques. *Fuel* **2005**, *84*, 859–867. [CrossRef]
30. Wang, X.; Huang, Z.; Kuti, O.A.; Zhang, W.; Nishida, K. Experimental and analytical study on biodiesel and diesel spray characteristics under ultra-high injection pressure. *Int. J. Heat Fluid Flow* **2010**, *31*, 659–666. [CrossRef]

31. Dent, J. A basis for the comparison of various experimental methods for studying spray penetration. *SAE Trans.* **1971**, *80*, 1881–1884.
32. Hiroyasu, H.; Arai, M. Structures of fuel sprays in diesel engines. *SAE Trans.* **1990**, *99*, 1050–1061.
33. Hiroyasu, H. Fuel spray penetration and spray angle in diesel engines. *JSAE* **1980**, *21*, 5–11.
34. Inagaki, K.; Mizuta, J.; Kawamura, K.; Idota, Y.; Hashizume, T. *Theoretical Study on Spray Design for Small-Bore Diesel Engine*; 0148-7191; SAE Technical Paper; SAE International: Warrendale, PA, USA, 2016.
35. Kitaguchi, K.; Matsumoto, M. Prediction of Diesel Spray with Super High Injection Pressure under High Atmosphere Density by Use of Experimental Formula and Numerical Simulation: 1st Report: Validity of the Experimental Formula Concerning the Spray Characteristics. *Symp. (ILASS-Jpn.) At.* **2012**, *21*, 15–22.

Disclaimer/Publisher's Note: The statements, opinions and data contained in all publications are solely those of the individual author(s) and contributor(s) and not of MDPI and/or the editor(s). MDPI and/or the editor(s) disclaim responsibility for any injury to people or property resulting from any ideas, methods, instructions or products referred to in the content.